ACS APPLIED MATERIALS & INTERFACES

Research Article

www.acsami.org

Influence of Source and Drain Contacts on the Properties of Indium–Gallium–Zinc-Oxide Thin-Film Transistors based on Amorphous Carbon Nanofilm as Barrier Layer

Dongxiang Luo,[†,‡] Hua Xu,[†,‡] Mingjie Zhao,[†,‡] Min Li,[†,‡] Miao Xu,*[,†,§] Jianhua Zou,[†,§] Hong Tao,[†,§] Lei Wang,[†,‡] and Junbiao Peng*[,†,‡,∥]

[†]Institute of Polymer Optoelectronic Materials and Devices, South China University of Technology, Guangzhou 510640, People's Republic of China

[‡]State Key Laboratory of Luminescent Materials and Devices, Guangzhou 510640, People's Republic of China

[§]School of Electronic and Information Engineering, South China University of Technology, Guangzhou 510640, People's Republic of China

[∥]Guangzhou New Vision Optoelectronic Co., Ltd., Guangzhou 510530, People's Republic of China

Supporting Information

ABSTRACT: Amorphous indium–gallium–zinc-oxide thin film transistors (α-IGZO TFTs) with damage-free back channel wet-etch (BCE) process were achieved by introducing a carbon nanofilm as a barrier layer. We investigate the effects of different source-and-drain (S/D) materials on TFT performance. We find the TFT with Ti/C S/D electrodes exhibits a superior performance with higher output current, lower threshold voltage, and higher effective electron mobility compared to that of Mo/C S/D electrodes. Transmittance electron microscopy (TEM) and X-ray photoelectron spectroscopy (XPS) are employed to analysis the interfacial interaction between S/D metal/C/α-IGZO layers. The results indicate that the better performance of TFTs with Ti/C electrodes should be attributed to the formations of Ti–C and Ti–O at the Ti/C-contact regions, which lead to a lower contact resistance, whereas Mo film is relatively stable and does not react easily with C nanofilm, resulting in a nonohmic contact behavior between Mo/C and α-IGZO layer. However, both kinds of α-IGZO TFTs show good stability under thermal bias stress, indicating that the inserted C nanofilms could avoid the impact on the α-IGZO channel regions during S/D electrodes formation. Finally, we successfully fabricated a high-definition active-matrix organic lighting emitting diode prototype driven by α-IGZO TFTs with Ti/C electrodes in a pilot line.

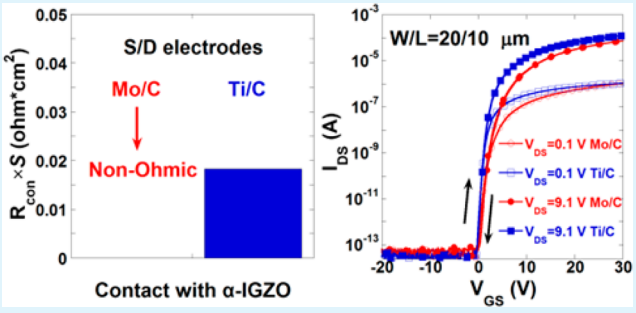

KEYWORDS: *thin-film transistors, amorphous-oxide semiconductor, contacts, carbon nanofilm*

1. INTRODUCTION

Since the report by Hosono et al., amorphous indium–gallium–zinc-oxide (α-IGZO) is of increasing interest for active material of thin-film transistors (TFTs) due to its high field-effect mobility, good uniformity, and excellent electrical stability.[1−4] After many years of studies, with the deeper understanding for material and process, the α-IGZO TFTs technology is gradually mature. Recently, many prototypes and products of active-matrix liquid-crystal display (AMLCD) and active-matrix organic lighting emitting diode display (AMOLED) driven by α-IGZO TFTs have been demonstrated.[5] However, compared with the widely used amorphous-silicon (α-Si) TFTs technology, the complicated process and relative high cost restricts the utilization of α-IGZO TFT technology.[6] As is known, amorphous-oxide-semiconductor (AOS) active materials, such as α-IGZO, α-IZO, etc., are very sensitive to most commonly used etchants and plasma bombardment,[4,6−10] therefore, the deposition of the source/drain (S/D) electrodes and the patterning of them will affect the electrical properties of α-IGZO TFTs, which results in the main difficulty of α-IGZO TFTs fabrication based on the back-channel-etch structure widely used in α-Si TFTs technology. Conventionally, by inserting an etch stopper layer between the α-IGZO and S/D electrodes, denoted as etch-stopper layer (ESL) structure, the impact on the active layer during the formation of the S/D can be greatly reduced. However, the use of ESL structure introduces two disadvantages: (1) an additional photolithography process is inevitably required, leading to a high production cost, and (2) it is difficult to achieve the miniaturization of TFTs due to the necessary

Received: November 13, 2014
Accepted: January 26, 2015
Published: January 26, 2015

DOI: 10.1021/am5079682
ACS Appl. Mater. Interfaces 2015, 7, 3633−3640

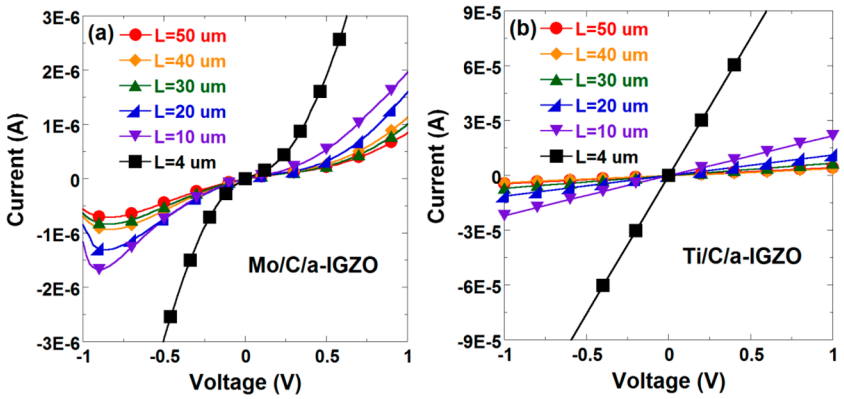

Figure 1. Current−voltage characteristics of (a) Mo/C/α-IGZO and (b) Ti/C/α-IGZO structures on glass substrates. Samples were annealed at 300 °C for 30 min in air.

overlapped regions in the ESL structure, which hinders the fabrication of displays with high resolution. To overcome these disadvantages of the ESL structure, the α-IGZO TFTs based on the back channel wet-etch (BCE) structure is being reconsidered now. The BCE structure in the bottom gated α-IGZO TFTs is featured because (1) the manufacture process step is simple, and compatible with the α-Si TFTs mass-production line, which means a higher yield and a lower equipment investment, respectively, and (2) it is easy to realize the miniaturization of α-IGZO TFTs and decrease the parasitic capacitance due to the smaller overlapping area between S/D and gate electrodes.

Recently, many efforts have been made on the achievement of high-performance α-IGZO TFTs based on BCE structure using a relatively low-cost and damage-free fabrication process.[6,11,12] Usually, both methods of wet etching by H_2O_2-based etchant and dry etching can be employed to pattern the S/D electrodes in AOS TFTs fabrication based on the BCE structure.[13−15] However, for the wet-etching process, the use of H_2O_2-based etchant introduces two disadvantages: (1) it has a short shelf life, and (2) especially, the H_2O_2 content has a possibility of explosion, so it is difficult to utilize the H_2O_2-based etchants in the mass-production process. Alternatively, dry etching could provide high etching selectivity between the S/D metal and the AOSs.[9] However, the plasma damage and the residual ions in the exposed AOS back surface during dry etching would cause the degradation of the AOS TFTs.[6,10] Additionally, special and expensive equipment is required for the dry etching process, which leads to increased production costs. Therefore, the achievement of high-performance AOS TFTs based on the BCE structure using a relatively simple process is drawing more and more attention.

In our previous study,[16] we introduced a sputtered amorphous carbon nanofilm as a barrier layer inserted into the interface between an amorphous indium−zinc-oxide (α-IZO) layer and S/D electrodes. We proved that a 3 nm thick C film is robust enough to protect the α-IZO channel from etching during the formation of the S/D electrodes by conventional wet-etching processes. In this work, the inserted C nanofilm is employed to fabricate high-performance α-IGZO TFTs with a BCE structure. The performance of α-IGZO TFTs with molybdenum and titanium S/D electrodes are investigated, respectively, because these metals are the most common electrode materials and often serve as contacting layer at the interface between low resistivity metal (such as Cu) and the semiconductor layer in the flat-panel-display technology. Furthermore, we give an insight on the interface reaction between S/D metals, C nanofilm, and α-IGZO layer, which explains the diversity of characteristics of C-inserted α-IGZO TFTs with BCE structure. Finally, we successfully fabricate a high-definition AMOLED prototype in a pilot line, proving that the BCE process has good application prospect.

2. EXPERIMENTAL SECTION

2.1. Device Fabrication. A 200 nm thick Mo layer was deposited onto glass substrates as a gate metal by dc magnetron sputtering and patterned by wet etching. Subsequently, a 250 nm thick Si_3N_4 layer and a 50 nm thick SiO_2 layer were formed successively by plasma-enhanced chemical vapor deposition (PECVD) acting as a gate insulator. The α-IGZO active layer with a thickness of 30 nm was deposited on SiO_2 by radio frequency (RF) magnetron sputtering, followed by wet etching in diluted hydrochloric acid. During the a-IGZO deposition, the flow rates of Ar and O_2 were kept at 20 and 2 sccm, respectively, and the power was fixed at 500 W. For the S/D electrodes, a stacked structure of Mo (200 nm)/C (3 nm) was sequentially formed by sputtering. The designed thickness of C film was estimated by multiplying the speed of growth and the sputtering time, and the actual thickness was checked via transmission electron microscopy (TEM). Then, a commonly used H_3PO_4-based etchant and oxygen (O_2) plasma were employed to pattern the Mo and C film, respectively.[16] The channel width (W) is 20 μm, and the channel length (L) is 10 μm. For comparison, α-IGZO TFTs based on Ti (200 nm)/C (3 nm) S/D electrodes were fabricated. Ti was patterned by a HF-based etchant, and C nanofilm was removed by the O_2 plasma as described above. Finally, all the devices were passivated by a 300 nm thick SiO_2 layer formed by PECVD and were annealed in air at 300 °C for 30 min.

2.2. Electrical Measurements. The current−voltage characteristics of the Metal/C/α-IGZO contacts and the electrical characteristics of the devices were measured by using a probe station and a semiconductor parameter analyzer (Agilent B1500). The negative bias temperature illumination stress (NBTIS) tests were performed for 2.5 h at V_{GS}= −20 V and V_{DS} = 0 V under a white light halogen lamp illumination with intensity of 1 mW/cm^2. The temperature was fixed at 60 °C during the stress evaluation, and the transfer characteristics were evaluated at a fixed V_{DS} of 9.1 V.

2.3. Characteristics of Carbon Nanofilms. The effect of the C nanofilms on the protection for the α-IGZO in the back-channel-etch process was analyzed via transmittance electron microscope (TEM, JEOL JEM2100F). The element distributions relevant to C nanofilms on actual device were depicted by using X-ray photoelectron spectroscopy (XPS, Thermo Scientific K-Alpha) and high-energy reflection electron energy-loss spectroscopy (EELS, Gatan).

DOI: 10.1021/am5079682
ACS Appl. Mater. Interfaces 2015, 7, 3633−3640

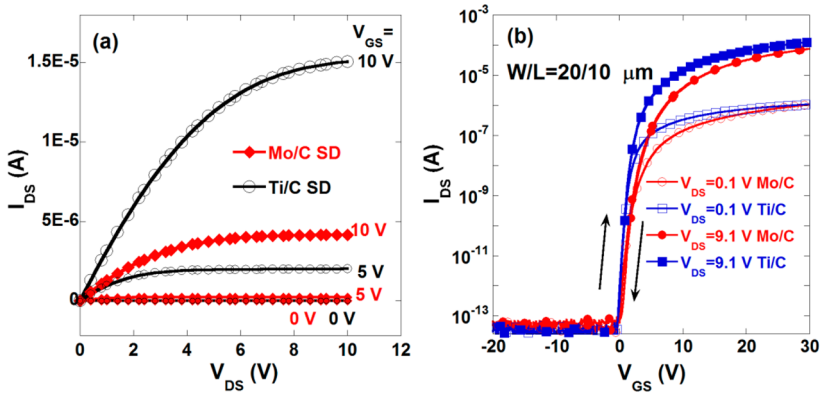

Figure 2. (a) Output characteristics and (b) transfer characteristics of the α-IGZO TFTs with Mo/C and Ti/C electrodes.

Table 1. Summarized Properties of the α-IGZO TFTs with Mo/C and Ti/C Electrodes

S/D electrodes	μ_{sat}	μ_{lin} ($cm^2\ V^{-1}\ s^{-1}$)	μ_{eff}	μ_i	*SS* (V/decade)	I_{on}/I_{of}	V_{th} (V)	V_{thi} (V)	R_cW (Ω·cm)	ΔV_{th} (NBTIS) (V)
Mo/C	7.3	8.6	7.0	7.1	0.35	4.3×10^9	4.5	4.9	300	−2.3/−0.2
Ti/C	12.5	14.1	10.2	9.8	0.24	1.1×10^9	2.4	3.6	135	−2.5/−0.1

3. RESULTS AND DISCUSSION

3.1. Influence of Carbon Nanofilm on the Contact Properties. First, we estimated the contact resistance between S/D electrodes and α-IGZO layer by the transmittance line model (TLM). The width (W) of metal pads was 200 μm and the distances (d) between pads were 4, 10, 20, 30, 40, and 50 μm. Prior to testing, all the samples were also annealed at 300 °C for 30 min in air, which is consistent with the manufacturing process of α-IGZO TFTs. Figure 1a,b shows the current−voltage (I−V) characteristics of Mo (200 nm)/C (3 nm) and Ti (200 nm)/C (3 nm) contact to α-IGZO, respectively. For the Mo/C/α-IGZO samples, the contact shows a nonlinear behavior, indicating a nonohmic contact between Mo/C and α-IGZO layer, whereas the Ti/C/α-IGZO contact exhibits a good linear I−V characteristics and a higher absolute I value, which suggests that the Ti/C/α-IGZO forms an ohmic contact and has a lower contact resistance (R_{con}) than that of the Mo/C/α-IGZO. In the TLM measurements, the total resistance (R_{tot}) between electrode pads is defined as the sum of the contact resistance R_{con} and the channel sheet resistance (R_{sq}). Here, the total device resistance R_{tot} is plotted as a function of the spacings of metal pads:

$$R_{tot} = R_{con} + R_{sq}d/W \quad (1)$$

where R_{tot} can be extracted from the I−V curves, and R_{con} can be deduced from the linear extrapolation of R_{tot} to the zero channel length. According to this formulation, we counted the R_{con} of Ti/C/α-IGZO is 0.018 Ω·cm^{-2}. To clarify the effects of C nanofilm on contact properties, we prepared the reference devices with Mo/α-IGZO and Ti/α-IGZO structures and then evaluated them by TLM. The corresponding I−V curves can be found in the Supporting Information. The devices with Mo/α-IGZO and Ti/α-IGZO structures both show a good ohmic contact behavior with contact resistivity of 0.087 and 0.035 Ω·cm^{-2}, respectively, which agrees with the previously reported results.[17] According to previous reports,[18] the superior contact property of Ti/α-IGZO structure should be attributed to the generation of a Ti−O phase, which generating oxygen vacancies and leading to increased carrier concentrations at the Ti/α-IGZO interface. Interestingly, when the C nanofilm was inserted into the metal/α-IGZO, the difference of the contact behavior between Ti/C/α-IGZO and Mo/C/α-IGZO was significantly enlarged, as shown in Figure 1a. The non-ohmic contact behavior of the Mo/C/α-IGZO was probably due to the barrier at the C/α-IGZO interface, thus producing Schottky barrier and increasing potential barrier height.[19,20] As for Ti/C/α-IGZO, however, smaller R_{con} (0.018 Ω·cm^{-2}) was extracted, which indicated that the C barrier at the Ti/C/α-IGZO contact is negligible. This result reflects that another contact mechanism exists at the Ti/C/α-IGZO interface. The analysis of equilibrium band diagrams of the stacked structures can be found in the Supporting Information.

3.2. Electrical Characteristics of α-IGZO TFTs with Metal/C Electrodes. Then, the TFT characteristics of the α-IGZO TFTs with Mo/C and Ti/C S/D electrodes were compared. Figure 2a shows the output characteristics (I_{DS} versus V_{DS}) of the two devices. It can be clearly seen that the α-IGZO TFT with Ti/C electrodes has higher output drain current (I_{DS}) than the device with Mo/C electrodes at the same V_{DS} and V_{GS}. The result indicates that the Ti/C has a higher efficient contact than the Mo/C electrodes, which is consistent with the contact-resistance measurement. The corresponding transfer characteristics of the α-IGZO TFTs are shown in Figure 2b. The TFT with Ti/C electrodes shows a subthreshold swing (SS) of only 0.24 V/decade, a threshold voltage (V_{th}) of 2.4 V, and an on-to-off current ratio (I_{on}/I_{off}) of larger than 10^{10}. Comparatively, the TFT with Mo/C electrodes shows a deteriorate subthreshold swing of 0.35 V/decade, a higher threshold voltage of 4.5 V, and a lower on-to-off current ratio of 4.3×10^9. However, both devices show negligible hysteresis between forward and reverse sweeps of the transfer curves, implying low defect density in the channel or at the gate insulator/channel interface.[21] It is worth noting that the field-effect mobility in linear regime (μ_{lin}) and in saturation regime (μ_{sat}) for the α-IGZO TFT with Mo/C electrodes are calculated to be only 8.6 and 7.3 $cm^2\ V^{-1}\ s^{-1}$, which are much lower than those of the device with Ti/C electrodes (14.1 and 12.5 $cm^2\ V^{-1}\ s^{-1}$), respectively. It is concluded that the performance of the α-IGZO TFT with Ti/C electrodes is

DOI: 10.1021/am5079682
ACS Appl. Mater. Interfaces 2015, 7, 3633−3640

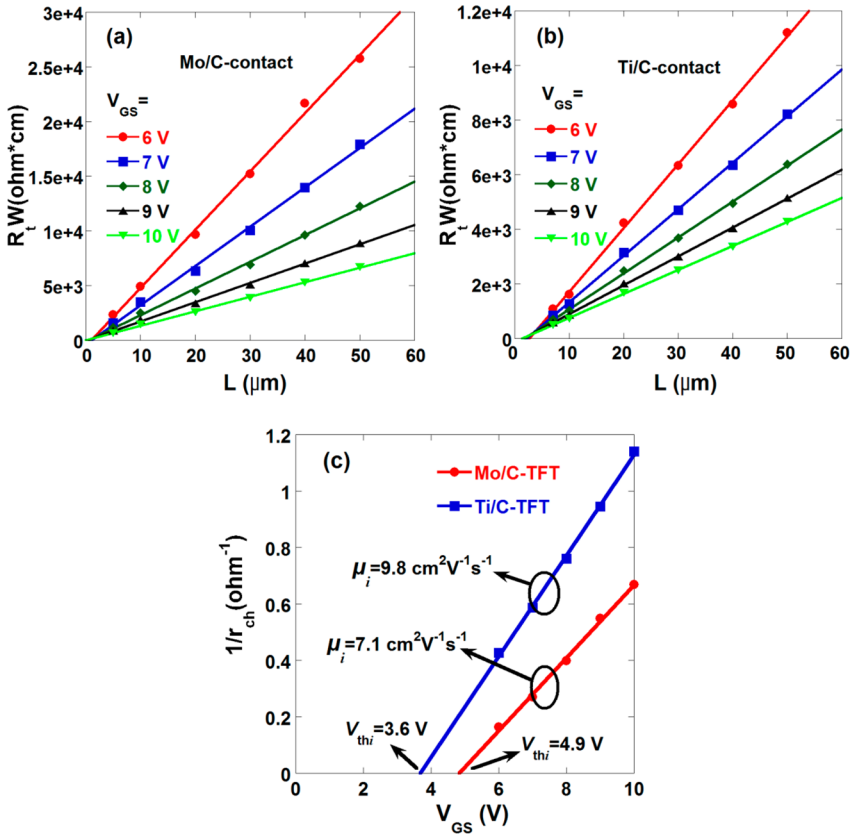

Figure 3. Dependence of R_tW on L for the α-IGZO TFTs with (a) Mo/C and (b) Ti/C contacts. (c) $1/r_{ch}$ versus V_{GS} plots for the α-IGZO TFTs with Mo/C and Ti/C contacts.

superior to that of the device with Mo/C electrodes. The properties of α-IGZO TFTs with Mo/C and Ti/C electrodes are summarized in Table 1.

It has been a common understanding that the electrical properties of the TFTs with different S/D electrodes are associated with contact resistances between the S/D electrodes and the semiconductor layer. Currently, the S/D contact resistance (R_c) can be evaluated by using the channel resistance method with TFTs having different channel lengths.[22] The total resistance (R_t) between source and drain electrodes is defined as the sum of the channel resistance (R_{ch}) and R_c by the following equations:[16,22]

$$R_t = R_c + R_{ch} \tag{2}$$

$$R_{ch} = r_{ch} \times L_{eff} = \frac{L - \Delta L}{\mu_i C_i W(V_{GS} - V_{thi})} \tag{3}$$

where r_{ch} is the channel resistance per channel length unit, and μ_i and V_{thi} are the intrinsic mobility and the intrinsic threshold voltage, respectively; C_i is the capacitance of the gate insulator; and ΔL is the difference between the effective channel length (L_{eff}) of fabricated TFTs and the design channel length (L). In performing R_c measurements, we chose a V_{DS} value as small as 0.1 V to minimize the drain voltage effect. By plotting the width-normalized total resistance (R_tW) as a function of L based on eq 2, R_c and ΔL can be estimated from the intersection point of the extrapolated linear fit of R_tW versus L plots. Figure 3a,b shows the R_tW versus L plots for the α-IGZO TFTs with Mo/C and Ti/C electrodes with W of 100 μm and L of 5, 10, 20, 30, 40, and 50 μm. The plots were performed at V_{GS} values of 6, 7, 8, 9, and 10 V, respectively. It can be seen that the width-normalized contact resistance (R_cW) is as high as 300 Ω·cm for the α-IGZO TFT with Mo/C electrodes compared to just 135 Ω·cm for the device with Ti/C electrodes, indicating that lower ohmic contacts are formed in the α-IGZO TFT with Ti/C electrodes. Moreover, ΔL was extracted to be 1.9 and 2.8 μm for TFTs with Mo/C and Ti/C electrodes, respectively. According to previous reports,[23] the shorter L_{eff} for AOS-TFTs was ascribed to etch bias or lateral diffusion of S/D dopant. By replacing L with L_{eff}, the effective mobility (μ_{eff}) was calculated to be 7.0 and 10.2 cm^2 V^{-1} s^{-1} for TFTs with Mo/C and Ti/C electrodes, respectively.

Furthermore, based on eq 3, by plotting the reciprocal of r_{ch} as a function of V_{GS} and fitting the results with a line, μ_i and V_{thi} can be deduced from the slope and x-intercept, respectively. As shown in Figure 3c, μ_i was extracted to be 7.1 and 9.8 cm^2 V^{-1} s^{-1} for TFTs with Mo/C and Ti/C electrodes, respectively. The corresponding V_{thi} was calculated to be 4.9 and 3.6 V for TFTs with Mo/C and Ti/C electrodes, respectively. Usually, the value of intrinsic parameters, such as μ_i and V_{thi}, should be irrelative to the S/D-electrode materials, because the model takes into account that part of the applied V_{GS} is dropped by the S/D contact resistance. However, it is noteworthy that the α-IGZO TFTs with the Ti/C electrode show a superior mobility and a more negative value of V_{th}, compared with that of TFTs with Mo/C electrode. The results suggest that the Mo/C- and Ti/C-contact at the S/D regions have completely different effects on the electrical properties of the α-IGZO TFTs with the BCE structure.

3.3. Analysis on the Effects of C-Barrier Layer on the Metal/C/α-IGZO Interface. High-resolution transmission electron microscopy (HRTEM) was employed to investigate

DOI: 10.1021/am5079682
ACS Appl. Mater. Interfaces 2015, 7, 3633−3640

the reason for the great difference between the a-IGZO TFTs with Mo/C and Ti/C S/D electrodes Figure 4a,c shows cross-sectional images of the α-IGZO TFTs with Mo/C and Ti/C electrodes in the contact regions, respectively. It can be seen that the C nanofilm, at the interface between α-IGZO and Mo films, exhibits a good continuity without any voids or peel-off even after annealing, which implies that the C nanofilm is reliable and stable as a barrier layer; comparatively, in the Ti/C/α-IGZO structure, the image exhibits a blurred boundary at the Ti/C interface, which implies that there is possible an interdiffusion effect between Ti and C after 300 °C annealing. On the other hand, the back channels of the α-IGZO TFTs with Mo/C and Ti/C electrodes were also investigated by using the HRTEM, as shown in Figure 4b,d. They clearly show that the back-channel surfaces of α-IGZO films are intact, even after patterning the S/D electrodes, which indicates that C nanofilm has a good corrosion resistance to protect α-IGZO channel from attacks caused by the commonly used Mo or Ti etchants during the formation of S/D electrodes. Moreover, there is no C residual layers are found at the α-IGZO back-channel surfaces, implying that C nanofilms can be efficiently eliminated by O_2-plasma. Therefore, it can be inferred that the different performance of the α-IGZO TFTs with Mo/C and Ti/C electrodes are not attributed to the contamination at the back channel. The above results reinforce the idea that the Mo/C- and Ti/C-contact have strong effects on the electrical properties of the α-IGZO TFTs.

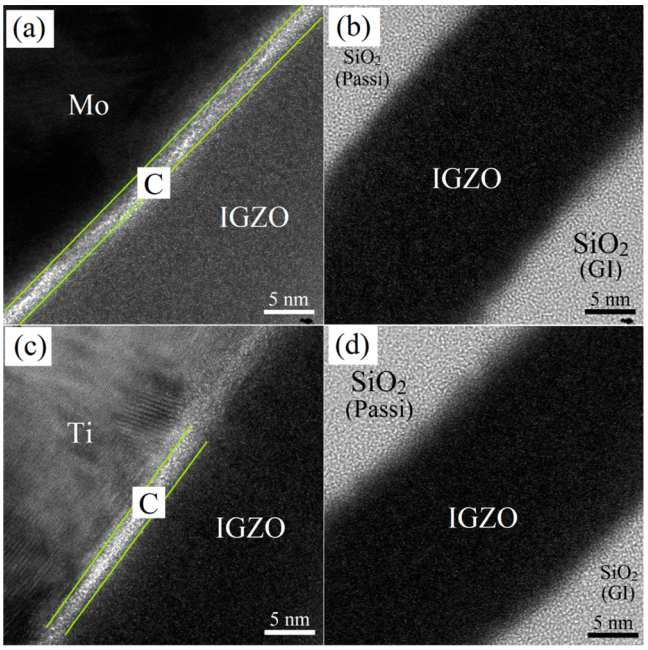

Figure 4. HRTEM cross-sectional images of α-IGZO TFTs with (a) Mo/C and (c) Ti/C electrodes in the contact regions. HRTEM cross-sectional view of α-IGZO TFTs with (b) Mo/C and (d) Ti/C electrodes in the channel regions. The devices were annealed at 300 °C for 30 min in air.

To further clarify the interaction between α-IGZO layer and electrodes with C nanofilm, X-ray photoelectron spectroscopy (XPS) depth-profile studies of the samples with metal/C/α-IGZO structure were carried out. In the experiments, samples of Mo(100 nm)/C(3 nm)/α-IGZO(50 nm) and Ti(100 nm)/C(3 nm)/α-IGZO(50 nm) were prepared on heavily doped

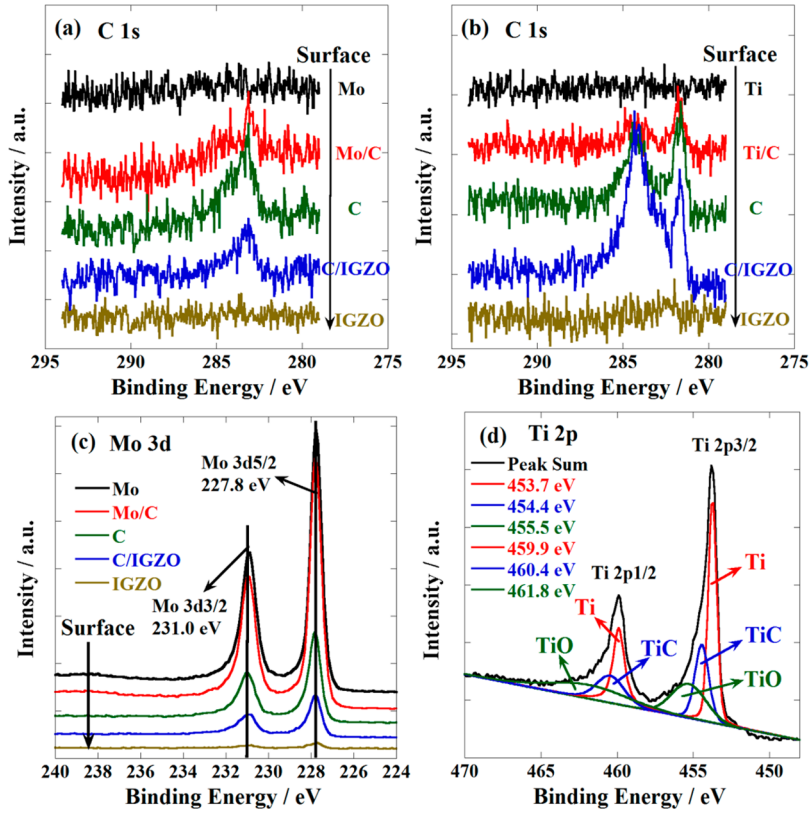

Figure 5. Depth profiles of XPS spectra for C 1s in (a) Mo/C/α-IGZO and (b) Ti/C/α-IGZO structures. (c) Mo 3d XPS spectrum at the Mo/C/α-IGZO interface. (d) Ti 2p XPS spectrum with the peak fitting at the Ti/C/α-IGZO interface.

DOI: 10.1021/am5079682
ACS Appl. Mater. Interfaces 2015, 7, 3633−3640

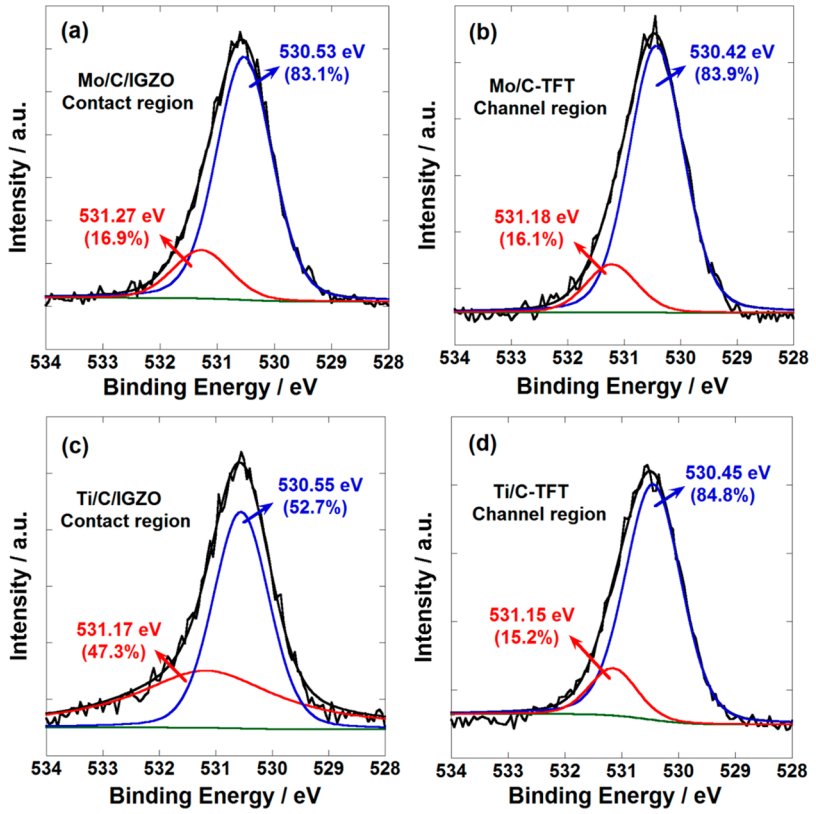

Figure 6. O 1s peak position of XPS spectra for α-IGZO films near the interface of the (a) Mo/C/α-IGZO and (c) Ti/C/α-IGZO contact regions, and O 1s peak position of XPS spectra for α-IGZO films near the surface of the (b) Mo/C- and (d) Ti/C-TFT channel regions.

silicon substrates, respectively. Meanwhile, to simulate the condition of the back channel of α-IGZO, the part of the samples was treated with metal etchants and O_2-plasma sequentially to eliminate the metal layer and C nanofilm. All the samples were annealed at 300 °C for 30 min in air. In the case of Mo/C/α-IGZO sample, the C and Mo XPS spectra at different depths are shown in Figure 5a,c. It can be seen that the C 1s peak is undetectable at the outset after the surface contamination was eliminated by using Ar ions at 500 eV for 10 s. With the increase of etching time, standard C 1s peaks located at 284.3 eV are detected at the interface between Mo and α-IGZO layer, implying only an isolated C element existed at the interface, even after annealing. Meanwhile, in the Mo 3d spectra, peaks are found at 227.8 and 231.0 eV, which confirms that there is not any carbon−molybdenum bond formation and only Mo metal existed at the Mo/C/α-IGZO interface.[24] On the other hand, in the case of the Ti/C/α-IGZO interface, C 1s peaks located at 284.5 and 281.8 eV were observed, as shown in Figure 5b. Among them, the peak with lower binding energy was relative to the values of C in carbide, indicating that there is some formation of Ti−C bonding at the Ti/C/α-IGZO interface after annealing.[25] Relatively, in the case of Ti 2p, however, the peak shape became more complicated. The doublet Ti $2p_{3/2}$ and Ti $2p_{1/2}$ peaks created by the spin−orbital interaction for Ti 2p are shown in Figure 5d. The Ti 2p3/2 peaks centered at binding energies of 459.9, 460.4, and 461.8 eV are related to free Ti element, Ti−C, and Ti−O, respectively.[26,27] Meanwhile, considering an energy difference of about 6 eV between both peaks of Ti 2p, the Ti 2p1/2 peaks with binding energy of 453.7, 454.4, and 455.5 eV correspond to free Ti element, Ti−C, and Ti−O, respectively.[26,27] The present results indicated that Ti would diffuse across the C barrier layer to reach the surface of α-IGZO film after annealing due to the formation of Ti−C, thus Ti−C could consume oxygen from the underlying α-IGZO and was oxidized into Ti−O.[18] In fact, it has been reported that the sensitivity of Ti toward oxidation was much higher than that toward carbonization.[27,28] It means that additional oxygen vacancies may be formed due to the formation of Ti−O. Therefore, more oxygen vacancies would be in existence at the Ti/C/α-IGZO interface.

Figure 6a,c shows the binding energy of O 1s XPS spectra in the α-IGZO layers near the interface of Mo/C/α-IGZO and Ti/C/α-IGZO, respectively. The peaks of ∼530.5 and ∼531.2 eV related to oxygen in oxide lattices without oxygen vacancies (O_L) and with oxygen vacancies (O_V), respectively, are found in both structures.[29,30] The relative area of the oxygen-vacancy peak, denoted as $O_V/(O_L + O_V)$, is calculated to be 16.9% in the Mo/C/α-IGZO sample, as shown in Table 2. Comparatively, in the case of Ti/C/α-IGZO sample, the ratio of O_V (47.3%) is much higher than that in the Mo/C/α-IGZO sample, indicating more oxygen vacancies are generated in the AOS layer when the Ti/C layer is employed as the S/D electrode material. Therefore, we speculate that a poor-oxygen

Table 2. Summary of the O 1s Peak Positions and the Relative Content of O_V for the α-IGZO TFTs with Mo/C and Ti/C Electrodes

samples	regions	O_L (eV)	O_V (eV)	$O_V/(O_L+ O_V)$ (%)
Mo/C/α-IGZO	contact	530.53	531.27	16.9
	channel	530.42	531.18	16.1
Ti/C/α-IGZO	contact	530.55	531.17	47.3
	channel	530.45	531.15	15.2

DOI: 10.1021/am5079682
ACS Appl. Mater. Interfaces 2015, 7, 3633−3640

region was formed in the α-IGZO layer under the S/D electrode region due to the oxidation of Ti/C contacts at the interface between α-IGZO and Ti/C electrode, leading to the lower contact resistance and superiority of mobility than α-IGZO TFTs with Mo/C electrodes. However, it is worth noting that the increase of oxygen vacancies in the α-IGZO channel regions always leads to instability in AOS TFTs under NBTIS test.[31,32] Therefore, we evaluated the density of oxygen vacancies near the surface of the α-IGZO at the back channel where the metal layer and C nanofilm were etched away. As shown in Figure 6b,d, we can find that the relative area of O_V (15.2%) in the α-IGZO film at the back channel of α-IGZO TFT with Ti/C contact is similar to that of α-IGZO TFT with Mo/C contact (16.1%), as shown in Table 2, indicating that the oxygen vacancy is not generated during deposition of Ti/C electrode but formed in the α-IGZO layer at the interface of Ti/C/α-IGZO structure after annealing. The result suggests that the both kinds of α-IGZO TFTs would display a comparative stability under NBTIS test due to the same level of oxygen vacancy.

3.4. Electrical Stability of α-IGZO TFTs with Metal/C Electrodes. To confirm the hypothesis, we characterized the electrical stability of the α-IGZO TFTs with Mo/C and Ti/C electrodes under NBTIS using a semiconductor parameter analyzer (Agilent B1500). For comparison, the α-IGZO TFTs with Mo and Ti electrodes were fabricated by dry etching using mixtures of SF_6/O_2 (Mo) and Cl_2/BCl_3 (Ti) as process gas, respectively. Both devices were annealed at 300 °C for 30 min in air after pattern the SiO_2 passivition layer, and the devices were also stressed under the identical stress condition. The detailed evolutions in transfer characteristics under NBTIS for the α-IGZO TFTs with metal/C and metal electrodes are shown in the Supporting Information, while the variations of the V_{th} shift as a function of the NBTIS time for the devices are shown in Figure 7. It can be seen that the V_{th} of the α-IGZO TFT with Mo/C electrodes shifts to the negative direction of about 2.3 V, and the device with Ti/C electrodes exhibits a similar negative V_{th} shift of about 2.5 V after the 2.5 h NBTIS application, indicating that the same amount of photoinduced electron−hole pairs creation in the channel. In addition, the dark stability of the devices with Mo/C and Ti/C electrodes under the same bias condition (NBTS) both exhibit a much smaller V_{th} (<0.2 V) shift in the negative direction than the stability with light illumination. These results showed that the formations of Ti−C and Ti−O at the Ti/C/α-IGZO interface have few effects on the NBTIS stability. On the other hand, the α-IGZO TFTs with Mo and Ti electrodes both exhibit tremendous V_{th} shifts in the negative direction, suggesting that a larger amount of photoinduced charge carrier is trapped under the electrical field, which might be involved with the formation of the byproducts or plasma damage during the dry etching process for pattering the Mo and Ti S/D electrodes.[8,9] From the above, we confirm that the existence of C nanofilms can not only protect α-IGZO layer from damage during formation of S/D electrodes in the BCE process, but also achieve the high-performance a-IGZO TFTs through optimizing the interface in the S/D region. Finally, we successfully achieved a 3.5 in. monochrome top emission AMOLED display driven by the optimized α-IGZO TFT with Ti/C electrodes in a pilot line (for details, see the Supporting Information), proving the feasibility of the BCE process.

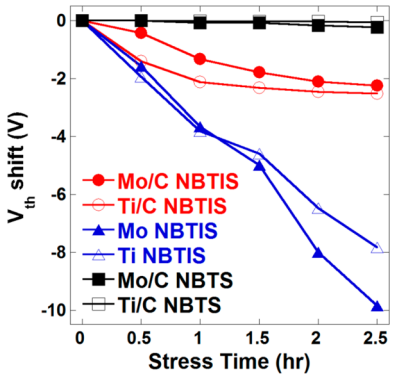

Figure 7. Variations of V_{th} shift under NBTIS for the α-IGZO TFTs with Mo/C, Ti/C, Mo, and Ti electrodes. In addition, the variations of V_{th} shift under NBTS for the α-IGZO TFTs with Mo/C and Ti/C electrodes are shown. The V_{th} values were evaluated from the *x*-axis intercept of the extrapolated linear fit of the sqrt (I_{DS}) vs V_{GS} plot.

4. CONCLUSIONS

In summary, a damage-free BCE process was achieved by introducing a C nanofilm as a barrier layer, and the influence of S/D electrodes on the performance of the α-IGZO TFTs was investigated. It was found the TFT with Ti/C S/D electrodes had higher I_{on}/I_{off}, lower V_{th}, and much higher μ_i than that with Mo/C S/D electrodes. TEM images revealed interdiffusion effects between Ti and C after 300 °C annealing. By using XPS depth profile analyzing method, we observed that the formations of TiC and TiO at the Ti/C-contact regions were the main reason for the better performance of TFTs with Ti/C electrodes. The excellent bias-thermal illumination stabilities further proved that the inserted C nanofilms could avoid the impact on the active layer during S/D electrode formation. Thus, the α-IGZO TFTs with double-layered Ti/C barrier layer would be a low-cost alternative for the AOS TFTs mass production.

■ ASSOCIATED CONTENT

Supporting Information

Current−voltage characteristics of Mo/α-IGZO and Ti/α-IGZO structures; analysis and schematic of estimated equilibrium band diagrams; EELS line scan analyses for the α-IGZO TFTs with Mo/C and Ti/C electrodes; bias stability of the α-IGZO TFTs with Mo/C, Ti/C, Mo, and Ti S/D electrodes; transfer characteristics of the α-IGZO TFTs with different C barrier thicknesses between metal/C electrodes and α-IGZO channels; and a 3.5 in. monochrome top emission AMOLED display driven by the corresponding α-IGZO TFT with Ti/C electrodes. This material is available free of charge via the Internet at http://pubs.acs.org.

■ AUTHOR INFORMATION

Corresponding Authors

* E-mail: xumiao4049@gmail.com.
* E-mail: psjbpeng@scut.edu.cn.

Notes

The authors declare no competing financial interest.

■ ACKNOWLEDGMENTS

The work was supported by MOST (Grant Nos. 2009CB930604, 317 2009CB623600, 2011AA03A110), NSFC (Grant Nos. 60937001, 61036007, 51173049) and the

DOI: 10.1021/am5079682
ACS Appl. Mater. Interfaces 2015, 7, 3633−3640

China Postdoctoral Science Foundation (Grant No. 2014M552197).

REFERENCES

(1) Nomura, K.; Ohta, H.; Takagi, A.; Kamiya, T.; Hirano, M.; Hosono, H. Room-Temperature Fabrication of Transparent Flexible Thin-Film Transistors using Amorphous Oxide Semiconductors. *Nature* **2004**, *432*, 488−492.

(2) Kim, H. S.; Park, J. S.; Jeong, H. K.; Son, K. S.; Kim, T. S.; Seon, J. B.; Lee, E.; Chung, J. G.; Kim, D. H.; Ryu, M.; Lee, S. Y. Density of States-Based Design of Metal Oxide Thin-Film Transistors for High Mobility and Superior Photostability. *ACS Appl. Mater. Interfaces* **2012**, *4*, 5416−5421.

(3) Bak, J. Y.; Yang, S.; Ryu, M. K.; Ko Park, S. H.; Hwang, C. S.; Yoon, S. M. Effect of the Electrode Materials on the Drain-Bias Stress Instabilities of In-Ga-Zn-O Thin-Film Transistors. *ACS Appl. Mater. Interfaces* **2012**, *4*, 5369−5374.

(4) Kwon, J. Y.; Lee, D. J.; Kim, K. B. Review Paper: Transparent Amorphous Oxide Semiconductor Thin Film Transistor. *Electron. Mater. Lett.* **2011**, *7*, 1−11.

(5) Kamiya, T.; Nomura, K.; Hosono, H. Present Status of Amorphous In-Ga-Zn-O Thin-Film Transistors. *Sci. Technol. Adv. Mater.* **2010**, *11*, 044305.

(6) Ryu, S. H.; Park, Y. C.; Mativenga, M.; Kang, D. H. Amorphous-$InGaZnO_4$ Thin-Film Transistors with Damage-Free Back Channel Wet-Etch Process. *Electrochem. Solid-State Lett.* **2012**, *1*, Q17−Q19.

(7) Kim, C. H.; Rim, Y. S.; Kim, H. J. Chemical Stability and Electrical Performance of Dual-Active-Layered Zinc−Tin-Oxide/Indium−Gallium−Zinc-Oxide Thin-Film Transistors Using a Solution Process. *ACS Appl. Mater. Interfaces* **2013**, *5*, 6108−6112.

(8) Kwon, J. Y.; Son, K. S.; Jung, J. S.; Lee, K. H.; Park, J. S.; Kim, T. S.; Ji, K. H.; Choi, R.; Jeng, J. K.; Koo, B.; Lee, S. The Impact of Device Configuration on the Photon-Enhanced Negative Bias Thermal Instability of GaInZnO Thin Film Transistors. *Electrochem. Solid State Lett.* **2010**, *13*, H213−H215.

(9) Kim, M.; Jeong, J. H.; Lee, H. J.; Ahn, T. K.; Shin, H. S.; Park, J. S.; Jeong, J. K.; Mo, Y. G.; Kim, H. D. High Mobility Bottom Gate InGaZnO Thin Film Transistors with SiO_x Etch Stopper. *Appl. Phys. Lett.* **2007**, *90*, 212114.

(10) Park, J. C.; Ahn, S.-E.; Lee, H.-N. High-Performance Low-Cost Back-Channel-Etch Amorphous Gallium−Indium−Zinc Oxide Thin-Film Transistors by Curing and Passivation of the Damaged Back Channel. *ACS Appl. Mater. Interfaces* **2013**, *5*, 12262−12267.

(11) Xu, H.; Lan, L.; Xu, M.; Zou, J.; Wang, L.; Wang, D.; Peng, J. High Performance Indium−Zinc-Oxide Thin-Film Transistors Fabricated with a Back-Channel-Etch-Technique. *Appl. Phys. Lett.* **2011**, *99*, 253501.

(12) Zhao, M.; Lan, L.; Xu, H.; Xu, M.; Li, M.; Luo, D.; Wang, L.; Wen, S.; Peng, J. Wet-Etch Method for Patterning Metal Electrodes Directly on Amorphous Oxide Semiconductor Films. *Electrochem. Solid-State Lett.* **2012**, *1*, P82−P84.

(13) Lee, S. H.; Seo, B. H.; Seo, J. H. Wet Etching of a Gallium Indium Zinc Oxide Semiconductor for Thin Film Transistor Application. *J. Korean Phys. Soc.* **2008**, *53*, 2603−2606.

(14) Luo, D.; Xu, H.; Li, M.; Tao, H.; Wang, L.; Peng, J.; Xu, M. Effects of Etching Residue on Positive Shift of Threshold Voltage in Amorphous Indium−Zinc-Oxide Thin-Film Transistors Based on Back-Channel-Etch Structure. *IEEE Trans. Electron Devices* **2014**, *61*, 92−97.

(15) Luo, D.; Li, M.; Xu, M.; Pang, J.; Zhang, Y.; Wang, L.; Tao, H.; Wang, L.; Zou, J.; Peng, J. Highly Stable Amorphous Indium-Zinc-Oxide Thin-Film Transistors with Back-Channel Wet-Etch Process. *Phys. Status Solidi RRL* **2014**, *8*, 176−181.

(16) Luo, D.; Zhao, M.; Xu, M.; Li, M.; Chen, Z.; Wang, L.; Zou, J.; Tao, H.; Wang, L.; Peng, J. Damage-Free Back Channel Wet-Etch Process in Amorphous Indium−Zinc-Oxide Thin-Film Transistors Using a Carbon-Nanofilm Barrier Layer. *ACS Appl. Mater. Interfaces* **2014**, *6*, 11318−11325.

(17) Hino, A.; Maeda, T.; Morita, S.; Kugimiya, T. Facilitation of the Four-Mask Process by the Double-Layered Ti/Si Barrier Metal for Oxide Semiconductor TFTs. *J. Inf. Disp.* **2012**, *13*, 61−66.

(18) Kim, H.; Kim, K.-K.; Lee, S.-N.; Ryou, J.-H.; Dupuis, R. D. Low Resistance Ti/Au Contacts to Amorphous Gallium Indium Zinc Oxides. *Appl. Phys. Lett.* **2011**, *98*, 112107.

(19) Huang, H. Y.; Wang, S. J.; Wu, C. H.; Chiang, C. K.; Su, J. Y. Performance Tuning of InGaZnO Thin-Film Transistors with a SnInGaZnO Electron Barrier Layer. *Appl. Phys. Lett.* **2013**, *102*, 092108.

(20) Gao, X.; Aikawa, S.; Mitoma, N.; Lin, M. F.; Kizu, T.; Nabatame, T.; Tsukagoshi, K. Self-Formed Copper Oxide Contact Interlayer for High-Performance Oxide Thin Film Transistors. *Appl. Phys. Lett.* **2014**, *105*, 023503.

(21) Kimura, M.; Nakanishi, T.; Nomura, K.; Kamiya, T.; Hosono, H. Trap Densities in Amorphous-$InGaZnO_4$ Thin-Film Transistors. *Appl. Phys. Lett.* **2008**, *92*, 133512.

(22) Chem, J. G. J.; Chang, P.; Motta, R. F.; Godinho, N. A New Method to Determine MOSFET Channel Length. *IEEE Electron Device Lett.* **1980**, *1*, 170−173.

(23) Sato, A.; Abe, K.; Hayashi, R.; Kumomi, H.; Nomura, K.; Kamiya, T.; Hosono, H. Amorphous In−Ga−Zn-O Coplanar Homojunction Thin-Film Transistor. *Appl. Phys. Lett.* **2009**, *94*, 133502.

(24) Lan, L.; Xu, M.; Peng, J.; Xu, H.; Li, M.; Luo, D.; Zou, J.; Tao, H.; Wang, L.; Yao, R. Influence of Source and Drain Contacts on the Properties of the Indium−Zinc Oxide Thin-Film Transistors based on Anodic Aluminum Oxide Gate Dielectrics. *J. Appl. Phys.* **2011**, *110*, 103703.

(25) Tachibana, T.; Williams, B. E.; Glass, J. T. Correlation of the Electrical Properties of Metal Contacts on Diamond Films with the Chemical Nature of the Metal−Diamond Interface. II. Titanium Contacts: A Carbide-Forming Metal. *Phys. Rev. B* **1991**, *45*, 11975−11981.

(26) Perry, S. S.; Ager, J. W.; Somorjai, G. A.; McClelland, R. J.; Drory, M. D. Interface Characterization of Chemically Vapor Deposited Diamond on Titanium and Ti-6Al-4V. *J. Appl. Phys.* **1993**, *74*, 7452−7550.

(27) Zhang, L.; Koka, R. V. A Study on the Oxidation and Carbon Diffusion of TiC in Alumina−Titanium Carbide Ceramics using XPS and Raman Spectroscopy. *Mater. Chem. Phys.* **1998**, *57*, 23−32.

(28) Leroy, W. P.; Detavernier, C.; Van Meirhaeghe, R. L.; Kellock, A. J.; Lavoie, C. Solid-State Formation of Titanium Carbide and Molybdenum Carbide as Contacts for Carbon-Containing Semiconductors. *J. Appl. Phys.* **2006**, *99*, 063704.

(29) Chong, E.; Jo, K. C.; Lee, S. Y. High Stability of Amorphous Hafnium−Indium−Zinc-Oxide Thin Film Transistor. *Appl. Phys. Lett.* **2010**, *96*, 152102.

(30) Jeong, S.; Ha, Y. G.; Moon, J.; Facchetti, A.; Marks, T. J. Role of Gallium Doping in Dramatically Lowering Amorphous-Oxide Processing Temperatures for Solution-Derived Indium Zinc Oxide Thin-Film Transistors. *Adv. Mater.* **2010**, *22*, 1346−1350.

(31) Ryu, B.; Noh, H. K.; Choi, E. A.; Chang, K. J. O-Vacancy as the Origin of Negative Bias Illumination Stress Instability in Amorphous In-Ga-Zn-O Thin Film Transistors. *Appl. Phys. Lett.* **2010**, *97*, 022108.

(32) Nomura, K.; Kamiya, T.; Hirano, M.; Hosono, H. Origins of Threshold Voltage Shifts in Room-Temperature Deposited and Annealed α-In-Ga-Zn-O Thin-Film Transistors. *Appl. Phys. Lett.* **2009**, *95*, 013502.

DOI: 10.1021/am5079682
ACS Appl. Mater. Interfaces 2015, 7, 3633−3640